Computational and Theoretical Chemistry 1205 (2021) 113443

Contents lists available at ScienceDirect

Computational and Theoretical Chemistry

journal homepage: www.elsevier.com/locate/comptc

# Applying transfer learning with convolutional neural networks to identify novel electrolytes for metal air batteries

Alfred Yan [a], Tatiana Sokolinski [c], William Lane [b], Jinwang Tan [b], Kim Ferris [d], Emily M. Ryan [b,c,*]

[a] Boston University, Department of Physics, Boston, MA 02215, U.S.A
[b] Boston University, Department of Mechanical Engineering, Boston, MA 02215, U.S.A
[c] Boston University, Division of Materials Science and Engineering, Boston, MA 02215, U.S.A
[d] Pacific Northwest National Laboratory, Computational Science and Mathematics Division, 902 Battelle Blvd, Richland, WA 99352, U.S.A

ARTICLE INFO

*Keywords:*
Lithium batteries
Convolutional neural networks
Ionic liquid crystals
Transfer learning

ABSTRACT

The formation of dendrites on the anode surface of metal air batteries, such as the Li-air battery, causes significant decreases in performance over the lifetime of the battery and poses safety concerns due to short circuiting. Predictive computational methods are used to investigate novel electrolyte materials which will reduce dendrite growth, in particular liquid crystal materials for Li-air electrolytes. The literature on liquid crystal electrolytes was surveyed for materials data and used to develop a training set of liquid crystal compounds. These compounds were then used as a knowledge base to develop property structure relations for the clearing and melting temperature for liquid crystals, which are a critical design parameter for the design of novel electrolytes. This was accomplished using standard artificial neural networks trained on molecular fingerprints and convolutional neural networks (CNNs) trained on compound images. Transfer learning was also demonstrated to boost predictive performance through pre-training neural networks on larger pre-existing compound datasets. The results show that CNNs achieve comparable accuracy compared to molecular fingerprints, and that both multilayer perceptrons and CNNs can benefit from transfer learning. This study is the first where transfer learning in CNNs aids in the prediction of one experimental property in a small data regime, using data of another experimental property.

## 1. Introduction

Metal air batteries, such as lithium air (Li-air) batteries, promise increased energy density and capacity compared to current battery systems, such as lithium ion (Li-ion) batteries. Li-air batteries have the potential to provide practical energy densities equivalent to gasoline (1,700 Wh/kg), and an order of magnitude greater than Li-ion batteries [1]. Li-air batteries are currently in the research and development stages for use as primary and secondary systems for portable and military applications and electric vehicles. Currently, state of the art research on Li-air batteries has demonstrated the reversibility of the system and has focused on modifying the materials and cell design to increase specific capacity and stability. Some of the key fundamental challenges in Li-air batteries include [2]: the formation of dendrites on the Li anode surface during cycling, increasing the electrochemical activity of the air cathode for both oxygen reduction and evolution reactions, and increasing the concentration and mobility of $O_2$ and $Li^+$ in the electrolyte. Together these challenges and others have limited the capacity of Li-air batteries and their cycle life.

Dendrite growth is a serious concern for Li-air batteries [2]. The growth of dendrites reduces the Li available for the electrochemical reactions and increases safety concerns due to short circuiting. Dendrite growth is a pernicious problem for electrochemical applications besides Li-air batteries, and has been observed for other battery chemistries, such as Li-ion and NiCd, and for many metal and electronic fabrication processes, such as solidification [3,4] and electroplating [5,6]. Research into methods for suppressing dendrite growth has considered everything from operating parameters [7,8] and novel physical separators [9–11], to new electrode [12–14] and electrolyte materials [15–18]. The success of any of these strategies has the potential to greatly increase the safety of Li-air batteries and increase performance by reducing Li loss with cycling. In this work we focus on the development of novel electrolyte

* Corresponding author.
*E-mail address:* ryanem@bu.edu (E.M. Ryan).

https://doi.org/10.1016/j.comptc.2021.113443
Received 22 January 2021; Received in revised form 28 August 2021; Accepted 3 September 2021
Available online 8 September 2021

materials as a possible solution to dendrite issues. Research into new electrolyte solutions for Li batteries typically involves experimental trial and error of possible materials, which can be a costly and time consuming process limited to known and available materials. Because of this, researchers have developed methods in which predictive machine learning models are trained to predict specific properties of candidate materials, which can be useful for screening a large dataset of materials for potential electrolytes [19–24]. There are several previous studies using this general method, which vary in the material database used, the specific material property that is optimized, and the types of machine learning models used [19,20,25–27]. Such studies include Ahmad et al [19], in which inorganic solid materials are screened for mechanical properties using a crystal graph convolutional network, and Ishikawa et. Al [27] in which coordination energies between different electrolyte solvents and ions are modeled using techniques including multiple linear regression and LASSO regression. To further this effort, large databases of battery-specific materials have been created [20,28–30], calculated from first principles calculations or by extracting from the literature.

In this study, we expand on previous research into machine learning and electrolytes, to consider the use of ionic liquid crystals (ILCs) for the electrolyte of Li-air batteries. As discussed in this paper, computational modeling of mass transport in Li-air batteries shows the potential for controlled mass transport to suppress dendrite growth [31]. ILCs are a class of materials that inherently demonstrate anisotropic properties and have the potential to be used for battery electrolytes [17,32].; however, as they are a smaller specialized subset of ionic liquids, which display a liquid crystal phase, there are not yet studies in the literature where machine learning is used to screen ILCs as battery electrolyte candidates, mostly because of a lack of high-volume data in the literature. Thus, in a step toward this goal, this study explores machine learning models that can reliably predict ILC properties in small-data regimes. In this work, a predictive computational framework is presented utilizing materials informatics for identifying promising ILCs as electrolyte solutions. By utilizing transfer learning, we extend the predictive capabilities of deep learning models on material properties relevant to new electrolyte development and small materials datasets.

## 2. Theory

Dendrite growth near the anode-electrolyte interface of Li-air batteries is a strong function of the mixing near the interface. Increasing the transport of Li ions through the electrolyte should suppress dendrite growth and extend the lifetime of Li-air batteries. To explore this theory smoothed particle hydrodynamics (SPH), a Lagrangian particle based modeling method, is used to model the physics of dendrite growth near the anode-electrolyte interface [31,33,34]. Using a previously developed SPH model of dendrite growth [31], the model is applied to investigate the effects of anisotropic transport properties on the growth rate and morphology of dendrites. As can be seen in Fig. 1, anisotropic diffusion ($D_y \gg D_x$ *and* $D_y \ll D_x$) decreases the rate of dendrite growth compared to isotropic diffusion.

Liquid crystals inherently have anisotropic transport properties in a liquid crystal phase (nematic, smectic, etc.) where their rod-like molecules are positionally ordered, which may allow for suppressed dendrite growth. Depending on the specific liquid crystal there will be a transition temperature between the phases, which will dictate the operating temperatures where this ordered, nematic phase will exist. To utilize this unique property of liquid crystals to induce anisotropic properties within an electrolyte, the transition temperatures of the liquid crystal would need to fall within the operating temperature range of the battery.

Using this basic theory, materials informatics techniques are used to explore the use of ILCs as possible electrolyte solutions for Li-air batteries. In particular, artificial neural networks are used to map structural features of ILCs to their transition temperatures. Artificial neural networks are a machine learning algorithm, where features of a dataset

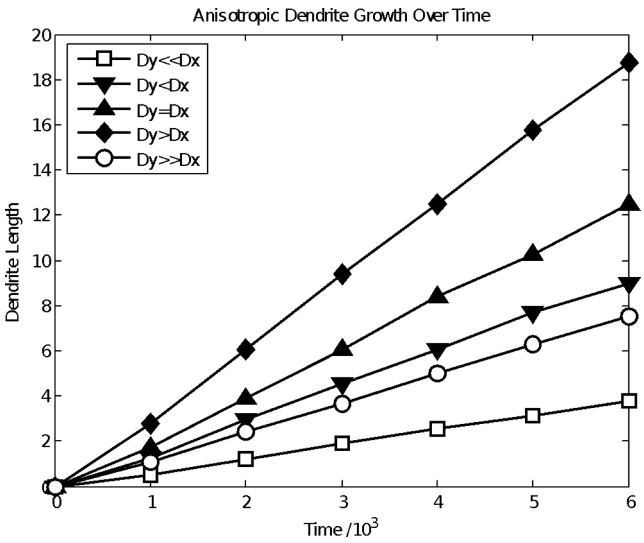


**Fig. 1.** Dendrite growth over time for several cases of isotropic and anisotropic diffusion where $D_x$ and $D_y$ refer to the diffusion rate through ($D_y$) the electrolyte and across the anode surface ($D_x$).

(such as structural features of relevant compounds) are mapped to an output space, which in this study is the ILC clearing and melting temperatures. This is done through successive forward-propagation steps and back-propagation steps—in forward propagation, features are passed as linear combinations to several nodes in a hidden layer, which then are linear combinations of the other nodes in the next hidden layer, etc. until a layer of nodes gets passed to one output value. Back propagation seeks to fit the neural network to the data by minimizing an error function like root-mean-squared-error (RMSE), which is done through updating parameters by calculating their derivatives of the cost function, a process known as gradient descent.

## 3. Methods

In this study, ILCs, particularly compounds that consist of an organic cation and an anion, are considered for Li-air electrolytes. Neural network models were used to predict clearing and melting temperatures, two relevant properties for electrolyte applications. The clearing temperature is a transition temperature between the isotropic liquid phase and the anisotropic liquid crystal phase, while the melting point is the transition temperature at which the ILC transitions during heating from a solid crystalline state to either a liquid crystal phase or an isotropic liquid, if there is no liquid crystal phase [32]. In our study, an ILC was still classified as an ILC even without a recorded liquid crystal phase, as long as it was included in other studies in tandem with other ILCs and had a similar structure. Two clearing temperature datasets were used, for which separate neural network models were developed: a larger mixed dataset of 230 clearing temperatures of various different cation types (imidazolium, guanidium, morpholinium, etc.), and a subset of that dataset consisting of 30 ammonium ILCs. Two melting temperature datasets were also used: a large set of 271 melting temperatures of ILCs of various cation types, as well as a subset of this dataset that consisted all the ammonium-based ILCs, containing 39 melting temperature data points, for which separate models were developed. One of the ammonium ILCs in the mixed dataset was not included in the ammonium dataset because the models consistently yielded inaccurate predictions for it, which will be elaborated on in the next section. To the authors' knowledge, there is no publicly available dataset containing a large amount of ILCs, so the datasets used were created by manually searching through publications from the literature [35–68]. Transition temperature data is provided in the Supporting Information.

Because of the small sizes of the datasets, in order to create a

predictive model, transfer learning was utilized. Transfer learning is a machine learning framework commonly used when the dataset in question (known as the "target" dataset) is too small of a size for developing an accurate model. In this study, in order to perform transfer learning, a neural network is first trained on another larger "source" dataset of a similar domain to create a "source" model, in a process called "pretraining", and then re-trained on the smaller target dataset in question, in a process known as "fine-tuning" [69]. Because the model was pre-trained, it can find a more accurate fit for the target dataset. Transfer learning was explored for this application by using different source tasks for the two different properties: for all our models, melting temperatures of ionic liquids were used to train the source model for fine-tuning afterwards. Melting temperature was used as the training source because the database contained 2212 data points for melting temperature [70]. For the clearing temperature models (for both the mixed and ammonium datasets) another source model was created by taking the model trained on the ionic liquid melting temperatures and fine-tuning it on the mixed dataset of ILC melting temperatures. Fig. 2 shows a schematic of the different source models used to train the target ILC clearing temperature model.

A similar method was used for training a model to predict ILC melting temperatures, creating a source model by taking a model trained on the 2212 ionic liquid melting temperatures and fine-tuning it on the mixed ILC clearing temperatures. The schematic for the different source models created to train a neural network on ILC melting points is shown in Fig. 3. Note that ILCs that were already in the collection of 2212 ionic liquid dataset were not included in our collection of 271 melting points.

For all datasets, two different types of models were used, multilayer perceptrons (MLPs) trained on molecular fingerprints of the ILCs, and convolutional neural networks (CNNs) trained on compound images, whose architecture and hyperparameters were determined empirically through intuition and trial-and-error. While generally hyperparameter search methods like grid search and random search are used for optimization, it was found that such methods were too computationally expensive for this study, given the need for many cross-validation (CV) repeats we performed, as will be explained in later sections. Thus, it was decided that using intuition would more suitably guide the study toward finding good hyperparameters. All models were developed using Keras with a TensorFlow backend [71]. The models' performance with and without transfer learning using both MLPs and CNNs was compared. The focus of interest in this investigation centered around the applicability of transfer learning with small datasets using CNNs. Transfer learning for molecular property prediction has already been well-documented in the literature, such as in Yamada et al [69] where improvements in performance was achieved by searching through a pre-made collection of candidate source models. In the ILC property prediction field, the use of "learned" representations via convolutions, whether on images or graph representations, is novel, as all published studies have used computable descriptors as neural network features. The most recent related study, performed by Low et al [72], compares the effectiveness of both ECFP4 and Coulomb matrix descriptors in ionic liquid melting point prediction. Such descriptors have demonstrated widespread success at prediction tasks, and are part of a trend in which hand-engineered features created by manually selecting functional groups to be represented as features are being substituted for more efficient featurizations like the aforementioned. Other molecular representations include using convolutions to "learn" suitable feature representations from scratch, which theoretically can be even more effective. Following this paradigm shift, CNNs were investigated because they have already shown potential in structure–property relations tasks in the drug discovery field, such as with Chemception, a CNN trained on images of drug-like molecules to predict properties like solvation energies, HIV activity, and toxicity [73]. Chemception was followed by Chemnet, where a CNN was first trained on 500,000 different molecules to predict values for their calculated molecular descriptors in a multitask setting, in order to learn general chemical trends, and then fine-tuned to predict a drug-relevant property using a smaller dataset [74]. There have been some other studies investigating the efficacy of transfer learning to increase CNN performance when training on molecular images, where source models have been well-established pre-trained models or were developed by training a large molecular database on easily computable properties [75,76]. However, in a materials science setting, it is useful to investigate whether transfer learning can be employed where the source task is one experimental property, and the target task is another, as neither the source nor target properties are guaranteed to have a large amount of experimental data in the literature. Furthermore, it is also worth investigating whether accurate CNN models can be created using extremely small datasets of a few hundred entries or less—to the authors' knowledge, the smallest molecular dataset that CNNs have been applied on so far is the Alpha-2a dataset containing 203 molecules [77]. There is some research on applications of CNNs on identifying liquid crystals, such as the study by Sigaki et al. [78] in which CNNs are used to identify the liquid crystal phase of microscope images of liquid crystals, but to the authors' knowledge, none have investigated them from a molecular property prediction framework that would allow for screening of new materials. There is potential in this area–if interpretability tools for CNNs are developed further, CNNs as molecular feature extractors may be used to highlight important substructures in a compound image that contribute to its predicted properties, yielding valuable structure–property insights.

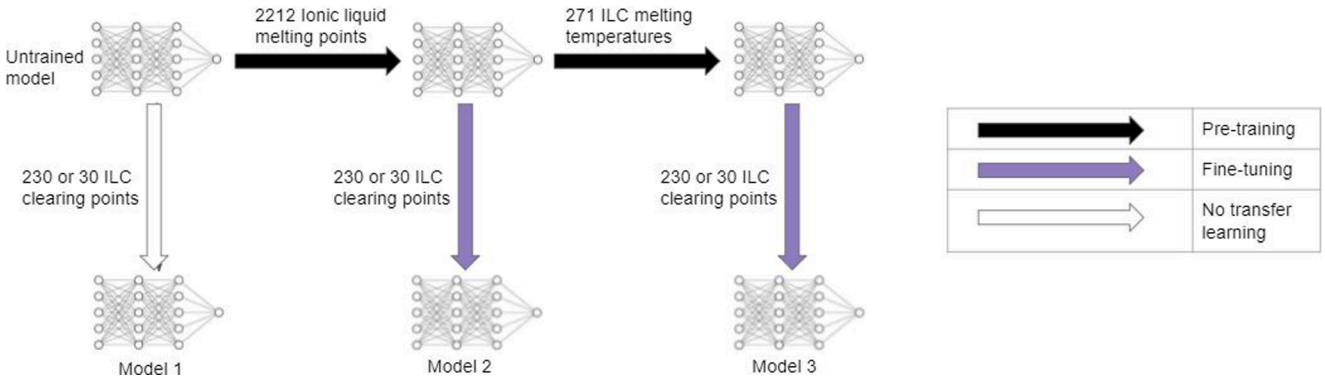


**Fig. 2.** Schematic of source models used for learning clearing temperatures–all paths starting from the *untrained model* to one of the bottom models (labeled Model 1, Model 2, or Model 3) represent how the neural network was pre-trained on different datasets before being trained on the representative melting temperature dataset. Two clearing temperature datasets were fitted: one consisting of a diverse array of 230 ILCs, and one consisting of 30 different ILCs, which is a subset of the mixed dataset consisting of ammonium-based cations. A newly-initialized model was trained on 2212 ionic liquids to create one source model. Another source model was created by training the ionic liquid source model on the dataset of ILC melting temperatures.

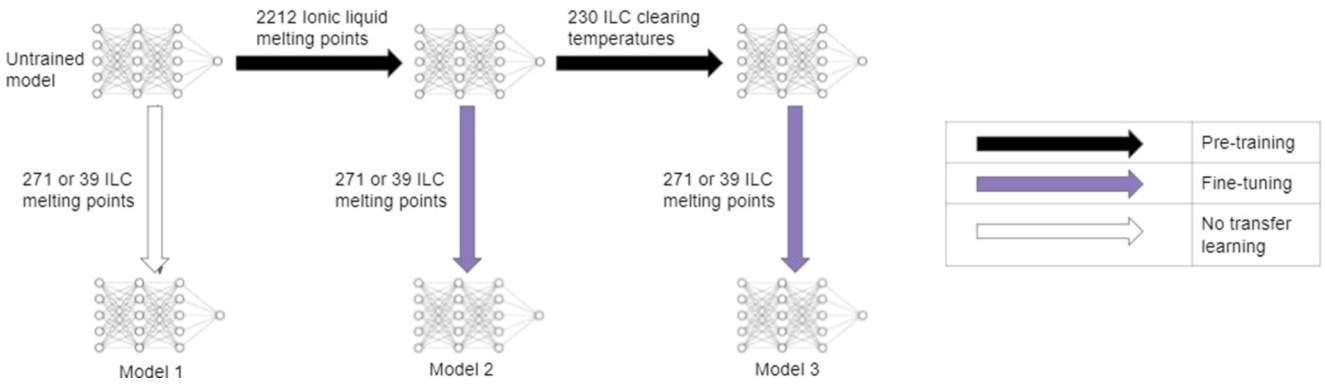


**Fig. 3.** Schematic of source models used to fit a neural network to ILC melting points—all paths starting from the *untrained model* to one of the bottom models (labeled Model 1, Model 2, or Model 3) represent how the neural network was pre-trained on different datasets before being trained on the representative melting temperature dataset. Two melting point datasets were fitted, one of size 271 consisting of a ILCs of diverse cation bases, and a subset of that dataset consisting of ammonium-based cations. One source model was created by training a newly-initialized model on 2212 ionic liquid melting points. Re-training that model on ILC clearing temperatures yielded another source model.

### 3.1. Multilayer perceptron

The performance of deep neural networks using molecular fingerprints was considered first. For all models, an architecture that consisted of 3 hidden layers of (100, 50, 20) neurons was used, using dropout with probability 0.1 only on the first hidden layer, and L2 regularization with $\lambda = 0.001$ on all hidden layers. Rectified Linear Unit (ReLu) was used as an activation function for the hidden layers. ECFP, MACCS, Atom Pair, rdkit, and Topological Torsion fingerprints were all explored using the Xenonpy python library [69]. It was found that the circular fingerprints were unusable, regardless of their radius, as several ILCs that were similar in structure (e.g. the only structural differences between some ILCs was the length of side carbon chains) had the same circular fingerprints. To achieve optimal performance, a concatenation of Atom Pair and Topological Torsion fingerprints were used. Low-variance features were removed in order to prevent overfitting. When performing transfer learning, one dataset (i.e. the target dataset, or one of the source datasets) was selected to have its columns with no variance removed, and the same features in the other datasets were removed accordingly. It was necessary to experiment with the datasets to find low-variance features to remove; for the mixed datasets, it was found that removing the low-variance features of the target dataset and then removing the corresponding source dataset features yielded superior performance. For the model trained on ammonium ILC clearing points, removing the no-variance features of the ionic liquid data yielded superior performance over removing low-variance features of the ammonium clearing point data. For the model trained on ammonium ILC melting temperatures, removing no-variance features (features where all the values are the same) of the ammonium melting point dataset yielded superior performance.

When training the model on the ionic liquid melting point dataset, the Adam optimizer was trained with a learning rate of 0.0001 for 200 epochs. When fine-tuning on the mixed datasets, the model was trained for 400 epochs using a learning rate of 0.001. When fine-tuning on the ammonium datasets, the dataset was trained for 300 epochs, again with a learning rate of 0.001. A batch size of 32 was used for all datasets; for learning ammonium clearing temperatures, where the dataset size was 30, this resulted in the model using the entire dataset in one batch. When performing fine-tuning, all layers were left trainable, as freezing layers did not lead to significant improvements. For the mixed dataset models, 20 iterations of 5-fold cross-validation were repeated in order to achieve stability and scores were calculated by averaging the $r^2$, MAE, and RMSE scores of all the folds across all 20 runs. The 20 repetitions were necessary because of the high variance of the models; the variance originated from both the small dataset size of the ILCs and the fact that there were "clusters" of similarly structured ILCs that originated from the same papers, which caused cross-validation scores to differ across different runs; while the process of repeating cross-validation 20 times was computationally expensive, it was found that the cross-validation scores of any model would consistently average to the same values, and so performance could be assessed reliably. For the smaller datasets of ammonium clearing and melting temperatures, leave-one-out cross-validation (LOOV) was used, repeated three times, and the average MAE, RMSE, and $r^2$ scores were calculated. It was found that when creating pre-trained source models for the ammonium ILC tasks, neural networks with the same architecture and hyperparameters trained on the same dataset could yield models that had varying effectiveness when used for transfer learning, due to randomness from shuffling data. Thus, different pre-trained models were created, and the scores recorded were the scores produced when using pre-trained models that yielded the optimal performance (i.e. had the lowest CV error and there was low variance in the 3 different CV scores).

### 3.2. Convolutional neural network

For the CNN, each ionic liquid and ILC was represented by a side-by-side concatenation of two 50x50x3 RGB images: one of the cation and the other of the anion, so that each compound was represented in total by a 50x100x3 image. These images were created through the rdkit python library using the MolstoGridImage function [79]. These image descriptors were chosen over the "chemception" image descriptors used by Goh et al. [73] because MolstoGridImage performed better. The differences between the two will be elaborated on in the Results and Discussion section. Different CNN architectures were used for the different datasets. For the mixed ILC datasets, the CNN architecture is as shown in Fig. 4.

For the ammonium datasets, fewer layers and parameters were employed in order to prevent overfitting, as shown in Fig. 5:

L2 regularization with $\lambda = 0.3$ and dropout with probability 0.3 was used on the fully connected layers. Hidden layers used the ReLu activation function. Convolutional layers used "same" padding, and Max-pooling layers used a stride length, (5x5), that was the same as the pool size. Data augmentation (transformations such as rotating each cation and anion image before concatenation) performed on each cation and anion image pair before concatenation was not used because it proved to be too computationally expensive, although it lead to a small increase in performance.

When performing transfer learning, a trial-and-error process of experimenting with freezing different layers revealed that for the mixed melting temperature datasets, the best performance was achieved by freezing the first convolutional layer while training all source models, while for the smaller datasets using the smaller architectures as well as

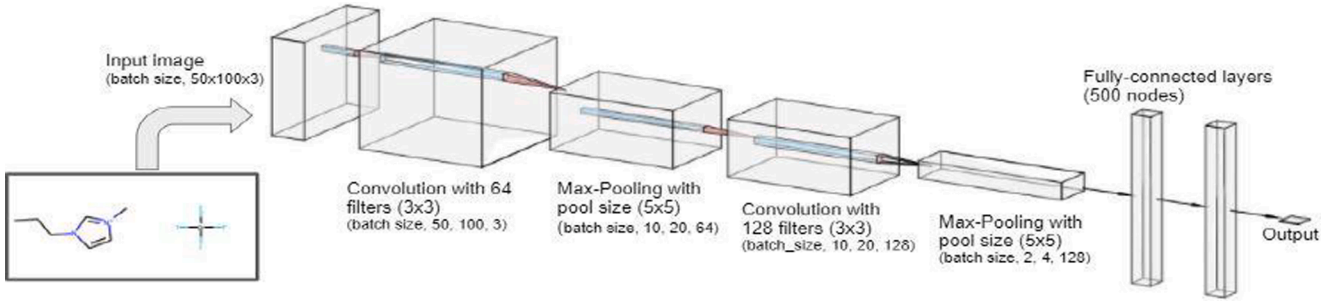


**Fig. 4.** CNN architecture used for the mixed ILC datasets of 230 clearing temperature data points and 271 melting temperature data points. For each ILC, a cation image was concatenated with an anion image before being fed into the network. Architecture hyperparameters were determined by trial-and-error and performances were assessed with repeated 5-fold cross-validation.

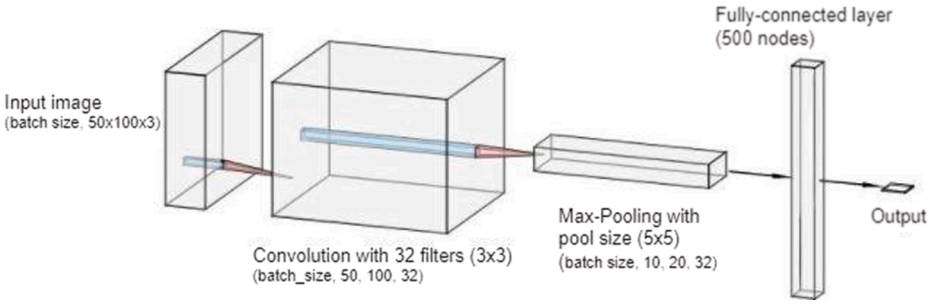


**Fig. 5.** CNN architecture used for the small ILC datasets of 30 clearing temperature data points and 39 melting temperature data points. A smaller number of layers were necessary to prevent overfitting. Performances were validated using leave-one-out cross-validation.

the mixed clearing temperature dataset, leaving all layers trainable yielded the best performance. The source model trained on the ionic liquids was trained using the Adam optimizer for 40 epochs with a learning rate starting at 0.001 that decayed by a factor of 0.1 every 5000 steps. A constant learning rate of 0.001 was used when fine-tuning on the mixed datasets, training for 500 epochs on ILC melting temperature data and 1000 epochs on ILC clearing temperature data. When fine-tuning to the ammonium datasets, the model was trained for 300 epochs. Batch sizes used were the same as in the multilayer perceptron models. Again, performance was validated using 5-fold CV repeated 20 times for the larger datasets, and LOOV repeated 3 times for the smaller datasets.

## 4. Results and Discussion

The performance of models trained on the mixed clearing temperatures is shown in Table 1. Performances of mixed melting temperatures, ammonium clearing temperatures, and ammonium melting temperatures are provided in the Supplemental Information.

Our models yield reasonable test performances; while our datasets had a relatively small size and contained a diverse selection of cation types, all MAEs were less than 30°. Our manually crafted ILC dataset has not been investigated elsewhere in the literature, so comparing our scores to a baseline is impossible. Nevertheless, it is possible to make an approximate comparison with other studies on ionic liquids. Namely, regression metrics of best performing models on the mixed ILC tasks from this study may be compared with scores found from other studies on predicting ionic liquid melting temperatures using the dataset of 2212 ionic liquids that was employed as a source model in this study. Our datasets are similar to this ionic liquid dataset in that both contain a diverse distribution of core structure types (e.g. imidazolium, pyridinium, etc). Thus, it can be expected that satisfactory performance metrics for the mixed ILC datasets should be comparable to those of the ionic liquid dataset. Following this, Table 2 presents a comparison of performance metrics. The $R^2$ scores of our study are very close to the top

**Table 1**
Performances of models trained on the large dataset of clearing temperatures, achieved through averaging the performance of all the folds after 5-fold cross-validation repeated 20 times. MAEs and RMSEs are in degrees Celsius. Both CNNs and MLPs were employed, and the CNN architecture is shown in Fig. 4. Performances of both methods were evaluated without transfer learning as well as with transfer learning having pre-trained on ionic liquid melting temperatures and ILC melting temperatures.

| | TRAINING | | TESTING | |
|---|---|---|---|---|
| Model | RMSE (MAE) | $R^2$ | RMSE (MAE) | $R^2$ |
| CNN without transfer | 5.6 (4.6) | 0.99 | 32.7 (23.8) | 0.59 |
| CNN with transfer from ionic liquid model | 6.0 (4.8) | 0.99 | 32.3 (24.6) | 0.60 |
| CNN with transfer from ILC melting temperatures | 5.4 (4.3) | 0.99 | 31.5 (23.5) | 0.62 |
| Fingerprints without transfer | 6.2 (4.7) | 0.99 | 34.1 (23.3) | 0.55 |
| Fingerprints with transfer from ionic liquid model | 7.1(5.8) | 0.98 | 31.1(21.9) | 0.63 |
| Fingerprints with transfer from ILC melting temperatures | 9.9 (8.52) | 0.96 | 29.5 (21.3) | 0.67 |

$R^2$ scores of Venkatraman et al. [80], the original study that produced the ionic liquid dataset. Our metrics are worse than those of Low et al. [72], who used ECFP circular fingerprints to predict ionic liquid melting temperatures. The reason that our study did not attain the same performance metrics could be because ECFP fingerprints were ineffective when tried on our dataset, and so different methods had to be implemented. For this reason, a direct comparison cannot necessarily be made between our ILC dataset and the ionic liquid dataset. Nevertheless, it is noteworthy that overall our study managed to achieve scores around the same range as what was achieved with a dataset almost a magnitude larger.

Regression metrics appear to be more favorable for the ammonium datasets. However, it is not certain that the models trained on the ammonium datasets necessarily are very useful; the majority of the

**Table 2**
Performance metrics of our dataset with that of other studies on the dataset of 2212 ionic liquids. The results of this study, which employed a datasets of size 230 and 271 ILCs, are loosely comparable to the results found in the literature on predicting ionic liquids of size 2212.

| | 230 ILC clearing temperatures (our dataset) | 271 ILC melting temperatures (our dataset) | 2212 ionic liquid melting temperatures (Venkatraman et al. [80]) | 2212 ionic liquid melting temperatures (Low et al. [72]) |
|---|---|---|---|---|
| $R^2$ | 0.67 | 0.66 | 0.67 | 0.74 |
| Mean Average Error | 21.3 | 14.4 | 33 | 29.8 |
| Root Mean Squared error | 29.5 | 22.3 | 45 | 39.8 |

cations in the dataset have very similar structures, which will likely lead to high bias when attempting to generalize to other ammonium ILCs, though the high performance metrics still indicate good accuracy when extrapolating to similarly structured ILCs. The training errors for the models trained on mixed datasets are all very low, which likely indicates overfitting. However, increased regularization and decreasing the number of model parameters techniques did not decrease the training error significantly and did not yield significant performance improvements.

In the ammonium datasets, one of the ILCs, 1,1,1-trialkyl-3,4,5-trialkyloxyanilinium tetrafluoroborate **1(8/BF$_4$)**, whose structure is shown in Fig. 6, was not included in the ammonium dataset. Only its melting temperature (161 °C) was found in the literature, which the ammonium models consistently gave poor predictions for, as shown in Table 3. The reason for this under prediction becomes apparent when inspecting literature data from Kuo et. Al [67] in Table 4. When comparing the transition temperatures of **1(8/BF$_4$)** with the other ILCs in the ammonium dataset whose structure only differed by alkyl chain length in the cation, it appears that crystal transition temperatures of **1(8/BF$_4$)** as well as the aforementioned model predictions are close to the melting temperatures of the other ILCs, but not the actual melting temperature of **1(8/BF$_4$)** itself. In fact, the melting temperature of **1(8/BF$_4$)** is anomalously high compared to the other ILCs. The model naturally extrapolated that the melting temperature of **1(8/BF$_4$)** would be close to the other melting temperatures, so its melting point prediction for **1(8/BF$_4$)** ended up in the same range as its crystal transition temperatures and far away from its true melting temperature. From merely inspecting the literature data in Table 4, it can be theorized that the mechanism behind melting in **1(8/BF$_4$)** is closer to the mechanism behind clearing than melting in the other ILCs because their temperatures are so close together, though the reason why such chemical differences arise is unknown. Had **1(8/BF$_4$)** not displayed such anomalous behavior and exhibited a liquid crystal phase in place of the two solid crystal phases it transitions to at 38 °C and 43 °C, it would have a melting point of either 38 °C or 43 °C. Then, model predictions would be more in-line. Overall, predictive models trained on literature data may not be robust against cases of ILCs that exhibit deviant thermotropic behavior, which is a problem that could also occur for predicting clearing temperatures, because there could also be ILCs with anomalous clearing temperatures that models may not be robust against. This is unlikely to be a fault in

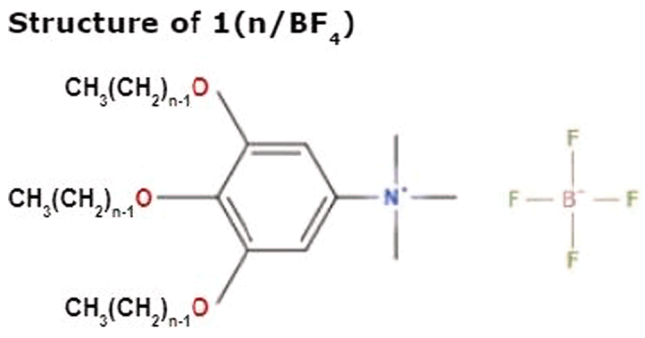


**Fig. 6.** Chemical structure of the **1(n/BF$_4$)** ILC.

**Table 3**
Predictions for the melting temperature of **1(8/BF$_4$)**, made by the best-performing models trained on the small dataset of ammonium ILCs.

| Model | Prediction (°C) | Error (°C) |
|---|---|---|
| CNN trained on ammonium ILCs | 32.4 | 128.6 |
| MLP trained on ammonium ILCs | 54.8 | 106.2 |

**Table 4**
Transition temperatures of 6 ILCs that were present in the ammonium dataset as well as the excluded **1(8/BF$_4$)**, taken from Kuo et al [67]. Recorded melting temperatures are bolded and clearing temperatures are shown with a *. Note that the melting temperature of **1(8/BF$_4$)** is in the same range of the clearing temperatures of the other ILCs. Cr = Solid crystalline phase, $Col_h$ = hexagonal columnar liquid crystalline phase, $Col_r$ = rectangular columnar liquid crystalline phase, Iso = isotropic liquid phase. The '1' and '2' designations refer to different morphologies of the liquid crystalline phase–further elaboration on liquid crystal behavior is found in the aforementioned references. Note how **1(8/BF$_4$)** does not display any liquid-crystalline behavior, and thus, its melting temperature is significantly higher than the others, leading to poor prediction performance for it.

| Value of n in **1(n/BF$_4$)** | Transition temperatures (°C) |
|---|---|
| 8 | Cr 38 Cr 43 Cr **161** Iso |
| 9 | Cr **29** $Col_{r2}$ 155 $Col_h$ 173* Iso |
| 10 | Cr **35** $Col_{r1}$ 59 $Col_{r2}$ 151 $Col_h$ 187* Iso |
| 11 | Cr **38** $Col_{r1}$ 63 $Col_{r2}$ 141 $Col_h$ 192* Iso |
| 12 | Cr **45** $Col_{r1}$ 87 $Col_{r2}$ 141 $Col_h$ 196* iso |
| 13 | Cr **47** $Col_{r1}$ 90 $Col_{r2}$ 130 $Col_h$ 197* Iso |
| 14 | Cr **53** $Col_{r1}$ 103 $Col_{r2}$ 134 $Col_h$ 196* Iso |

hyperparameter and architecture selection, but rather that existing models in the literature as well as in this study have not been developed to predict the specific thermotropic behavior such as the number of different phases and the different types of phases of an ILC. Further investigations in this area could therefore address this problem by creating models that simultaneously predict all the transition temperatures of a compound as well as their associated phases, instead of being limited to predicting one specific transition temperature.

For most models, transfer learning brought performance improvements. When the larger ILC datasets were the target task (i.e. pre-trained models were fine-tuned on the larger ILC datasets of size 230 or 271), there were mixed results, and transfer learning led to larger performance improvements when fingerprints were employed over CNNs, as seen in Fig. 7. While the improvements seen using CNNs are small, it is likely that they are due to using the pre-trained weights, as the 20 cross-validation repetitions would have canceled out many differences due to stochastic processes and instabilities from random shuffling while cross-validating. On the other hand, when observing the results from training on the ammonium datasets, CNNs uniformly saw higher differences in performance between models with and without transfer learning, as shown in Fig. 8.

When comparing transfer learning using a source model trained on ILC properties versus using a source model trained on ionic liquid melting points, using a source model trained on the opposite ILC property almost always yielded slightly greater improvements over transfer

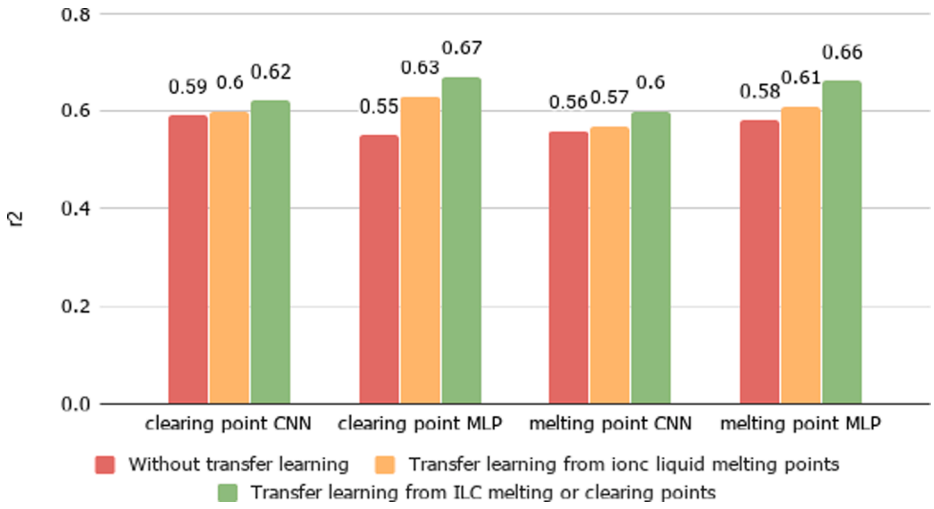


**Fig. 7.** Graph of model performances trained on datasets of ILCs of various cation types, with and without transfer learning. Transfer learning with molecular fingerprints yields greater improvements than with CNNs and has the best performance overall.

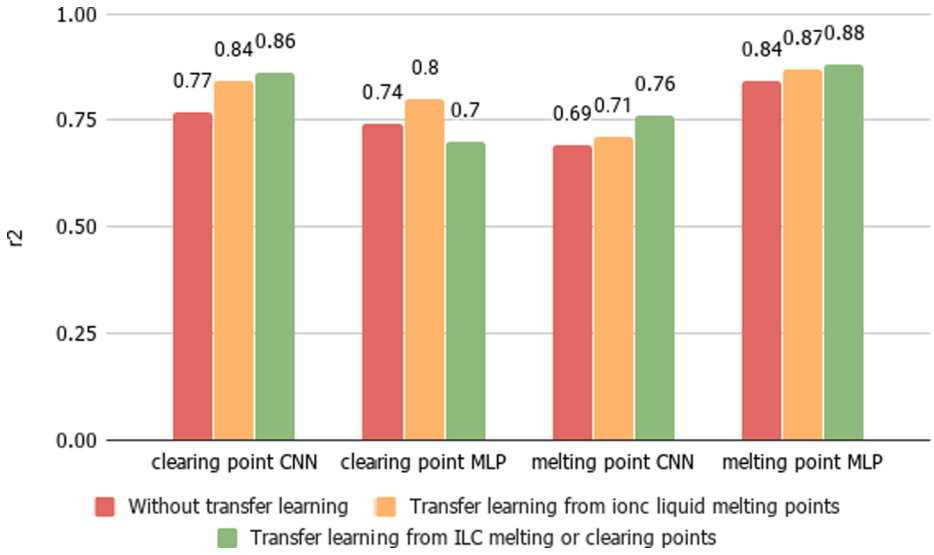


**Fig. 8.** Graph comparing model performances trained on small-sized datasets of ammonium-based ILCs. For the ammonium-based ILCs, CNNs show greater performance differences between training with and without transfer learning than standard neural networks (Fig. 7). However, when comparing final scores for the ammonium ILCs, CNNs only outperform fingerprints in predicting clearing temperatures.

learning using the ionic liquid melting temperature source model, except in the ammonium clearing temperature model trained on fingerprints. This can also be seen in Figs. 7 and 8. This trend is not unexpected, as training a source model on ILC data already teaches the neural network important structural information on the ILCs for the target task. However, while using the models to extrapolate to ILCs outside of the test domain, the models pre-trained on ILC properties may not necessarily outperform models pre-trained on the ionic liquid melting points, since models pre-trained on ILC properties may be overfitted on ILCs in the dataset, and for ILCs that have structural properties that differ from those in the ILC dataset, models pre-trained on ionic liquid melting temperatures may perform better. The reason the ammonium clearing temperature model does not follow this trend is unclear. In fact, there was negative transfer (where using pre-trained weights decreased performance) when transferring from ILC melting points to ammonium ILC clearing points, which is unexpected since the source domain of ILC melting points was not expected to be radically different from that of ammonium clearing points. It is not clear why this occurred, and negative transfer is a recent field of study in machine learning whose causes are an active area of investigation [81]. It may be that because the ILC melting temperature dataset contains ILCs that are not in the clearing temperature dataset, the neural network learns features that are inversely correlated or unrelated to clearing temperatures of the ammonium ILCs. However, this is merely speculative, and there could also be other stochastic processes that are influencing performance, which are currently unknown and may be subject to future studies. These exceptions to the trend reveal that intuition alone is not enough to definitively reveal which source models will be useful for a certain target task, and that it is useful to create as many source models as possible and test them individually to maximize performance—despite negative transfer from ILC melting points, transfer learning still brought performance improvements for the ammonium clearing temperature dataset when pre-trained on ionic liquid melting points.

With a few exceptions, CNNs appear to generally underperform compared to molecular fingerprints. Generally, when using molecular fingerprints, transfer learning appears to bring more improvements, and there are clearer differences in performance when using different source

models. Furthermore, fingerprints lead to more desirable scores in almost all models. This result is unsurprising, and is in-line with the hypothesis that CNN models need larger data sets in order to learn chemical features. Furthermore, in our CNN models data augmentation was not used; data augmentation is a commonly used technique when training CNNs, where input images undergo certain transformations like a random rotation or reflection. This process allows CNNs to become more robust by learning features regardless of their initial orientation on the image, and was employed in the development of Chemception and Chemnet mentioned in Section 3. While data augmentation appeared to yield small increases in performance in this study, it was not employed due to its computational cost. The image processing during data augmentation would drastically slow down the time needed for the models to converge, and combined with the need to train on 20 different cross-validation shuffles for our mixed datasets, data augmentation became impractical. Despite this setback, one exception where CNNs slightly outperform molecular fingerprints is when predicting ammonium ILC clearing temperatures. This is surprising, as it was expected that CNNs would perform poorly universally. This may be because when preprocessing low-variance features of the fingerprint vectors, the amount of data points (30) is significantly smaller than the feature vector length (4636 columns), which causes overfitting. However, different fingerprint algorithms and different variance thresholds when removing low-variance columns were experimented with, which all yielded approximately the same or worse performance, so this is not a particularly strong explanation. Another possible explanation is that because many ammonium ILCs in the datasets had a very large molecular size, as shown in Fig. 9, and emergent properties like transition temperatures start to depend on the overall shape of the ions, computer vision techniques, such as CNNs, are more adept at capturing them. Further investigation on the efficacy of CNNs could be in this area, and it may be worth testing CNN performance on small datasets of other complex compounds beyond ILCs to see if CNNs perform better for complex molecules overall. Currently, however, the exact mechanisms are unclear, especially since CNNs underperformed at all the other tasks. Overall, while CNNs underperformed compared to molecular fingerprints, this is a rather expected outcome, given how CNNs usually need larger datasets to learn raw chemical and structural properties; if large ILC datasets become available containing tens of thousands of data points, the comparative performance of CNNs may be worth revisiting.

As an ablative study, the effect of image blurring, which decreases the spatial resolution of the images, is investigated on model prediction power. Although common sense would dictate that blurring the image would decrease predictive power, from a chemical standpoint, this may be a compelling study because blurring may force the models to learn holistic structures of the molecules instead of analyzing individual atoms and bonds. In this study, a Gaussian blur of different kernel sizes is applied to the images using the OpenCV python library [82] and then trained on the ammonium ILC melting temperature task without transfer learning. The value of sigma of the Gaussian blur is calculated as being dependent on the kernel size n, using Equation (1):

$$\sigma = 0.3\left(\sqrt{n-1}-1\right)+0.8 \tag{1}$$

The performance metrics are displayed in Table 5.

It is clear that Gaussian blurring monotonically decreases model performance, negating the earlier hypothesis regarding learning holistic structures. Thus in order for a model to perform effectively, the images should keep a high resolution and display as many details about the molecule as possible.

Finally, we compare the differences in performance of images created from the MolstoGridImage function in rdkit with the image descriptors introduced in Chemception, which will be referred to as "chemcepterizations", which we copy exactly as described in the Chemception study by Goh et al. [73] In order to "chemcepterize" a molecule, the 2-D coordinates of the atoms are plotted on a dark background: pixels where atoms are located are given a value equal to the atomic number of the atom, and bonds between atoms are drawn as lines, with pixels representing a section taking a value equal to 2. This is because 2 is the atomic number of helium, which is not present in any of the molecules in the datasets used, so the number 2 can be used as a unique representation for the chemical bonds. Chemcepterized images of size 50x100 (the same as for MolstoGridImage) were created and used for the ammonium tasks. Overall, these chemcepterized images struggle to match the performance of MolstoGridImage. As an example, performance metrics for the ammonium ILC melting temperature task is included in Table 5 in the Supplementary Material. This is unexpected but not too surprising, as MolstoGridImage contains approximately the same amount of chemical information as chemcepterizations. Images created by MolstoGridImage are similar to chemcepterized images in that in MolstoGridImage, different elements in the molecules are given a unique color, analogous to different atomic numbers used by chemception. MolstoGridImage also draws double bonds, unlike chemcepterization which only uses the number 2 for all bonds. The only information that chemcepterization includes that MolstoGridImage does not is the exact atomic numbers, as MolstoGridImage picks an arbitrary color and thus an arbitrary value for different elements, yet this advantage may end up being irrelevant if the goal of the model is to learn to differentiate molecular structures. Futhermore, chemcepterizations may suffer from sparsity more than MolstoGridImage. For example, if an anion consists of only one atom, such as bromide, then it is represented by one pixel in its entire size 50x50 image representation, increasing the model's risk of overfitting. In contrast, MolstoGridImage creates a traditional structural diagram of the molecule, where atoms are represented by their chemical symbol and thus take up more space on the image. At the same time, the inferior performance of chemcepterizations may be because the 50x100 sizes of the images are too small, negatively

**Table 5**
Different filters are used on the ammonium ILC images before being used for to the melting temperature task. Gaussian blurring is seen to monotonically decrease performance.

| Kernel Size (n × n) | No filter (baseline) | 3 | 5 | 7 | 9 |
|---|---|---|---|---|---|
| $R^2$ | 0.69 | 0.55 | 0.43 | 0.39 | 0.36 |
| Mean Squared Error | 10.0 | 11.7 | 13.7 | 14.2 | 14.5 |
| Mean Average Error | 12.4 | 14.9 | 16.6 | 17.3 | 17.8 |

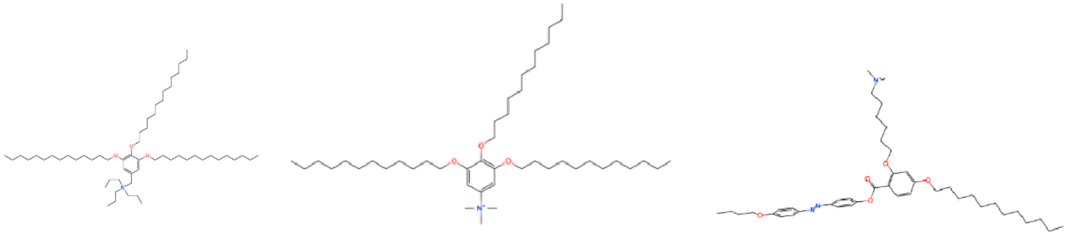

**Fig. 9.** Several different cations of ammonium-based ILCs. The large size and complexity of these cations may be a driving factor for the superior performance of CNNs over molecular fingerprints.

affecting the resolution as too many atoms are crammed into a few pixels. However, increasing the image size and therefore resolution did not improve performance, so this hypothesis is not particularly compelling.

## 5. Conclusion

This study is the first known example where transfer learning has been conducted with CNNs to aid in the prediction of one experimental property using data of another experimental property, applied to small dataset sizes realistically encountered in chemistry problems. While there was more difficulty in yielding very large differences in model performance through transfer learning with CNNs than with molecular fingerprints, there were still concrete improvements when using CNNs that hint at the possibility of utilizing transfer learning more effectively in other studies. Furthermore, molecular fingerprints have been demonstrated to reliably yield significant performance improvements through transfer learning, and the results of this study show that different transition temperatures have "related" domains that are transferrable to each other. Thus, it may be worthwhile to investigate the efficacy of transfer learning on other transition temperatures, like glass transition temperatures and decomposition temperatures, for which data is scarcer.

There are several takeaways on improving the predictive abilities of CNNs. One is the need for computing power; image processing methods like data augmentation can drastically slow down the training process by an order of magnitude, at which point the availability of computational resources becomes a bottleneck. Small dataset sizes can also lead to increase instability, necessitating the need to repeat cross-validation many times. This study did not use data augmentation for these reasons. Furthermore, multi-task transfer learning was not employed to first predict computable chemical descriptors of the chemicals in the dataset before fine-tuning to the target tasks, as described in Chemnet. This is because the authors were interested in the ability of CNNs to learn raw transferable features between experimental properties without the aid of engineered descriptors. It may be possible that using such a technique, combined with transfer learning between different experimental properties, would bring CNN performance to be on-par with fingerprints. However, this is not done easily–for this specific study, this would be best implemented with a large dataset of thousands of different unlabeled organic cations and anions for pre-training, which to the authors' knowledge does not yet exist.

While this study investigated applications of CNNs and molecular fingerprints, current paradigms in computational chemistry/materials science are geared towards applications of Graph Convolutional Networks (GCNs), with the emergence of MoleculeNet, a quantitative structure property relationship (QSPR) study which revealed the superior performance of several different GCN algorithms over molecular fingerprints [83]. When applied to ILC transition temperature tasks, GCNs may have mixed performance, especially GCN algorithms that involve analyzing the radial paths in a molecular graph. An example of this is that developed by Duvenaud, et al [84]. This is because they may have difficulty in differentiating compounds with the same core structure but varying lengths of alkyl chains, a problem that appeared when attempting to use circular fingerprints on the ILCs in this study. However, GCNs are a very active field of research and there are various approaches to molecular graph convolutions, so future studies could still investigate their performance on ionic liquid crystal property prediction tasks. GCN and CNN performances both rely on large datasets to learn raw chemical features, and their performances will likely improve relative to molecular fingerprints in the future as dataset sizes grow. While it is unclear whether CNNs will catch up to molecular fingerprints in the future, there may be a niche for CNNs in learning properties of large, complex molecules if it is true that they perform better than molecular fingerprints in such tasks.

## CRediT authorship contribution statement

**Alfred Yan:** Conceptualization, Methodology, Software, Investigation, Data curation, Writing – original draft, Visualization. **Tatiana Sokolinski:** Methodology, Investigation. **William Lane:** Writing – original draft, Investigation, Formal analysis. **Jinwang Tan:** Software, Formal analysis, Visualization. **Kim Ferris:** Conceptualization. **Emily M. Ryan:** Conceptualization, Writing – original draft, Writing – review & editing, Supervision, Funding acquisition.

## Declaration of Competing Interest

The authors declare that they have no known competing financial interests or personal relationships that could have appeared to influence the work reported in this paper.

## Acknowledgments

This research was partially supported by Samsung Electronics Company through the Samsung GRO Program, Boston University's Undergraduate Research Opportunities Program, and the National Science Foundation through a supplemental Research Experience for Undergraduates award to CMMI award 1727316.

## Appendix A. Supplementary material

Supplementary data to this article can be found online at https://doi.org/10.1016/j.comptc.2021.113443.

## References

[1] G. Girishkumar, B. McCloskey, A.C. Luntz, S. Swanson, W. Wilcke, Lithium–Air Battery: Promise and Challenges, J. Phys. Chem. Lett. 1 (14) (2010) 2193–2203, https://doi.org/10.1021/jz1005384.
[2] J. Christensen, P. Albertus, R.S. Sanchez-Carrera, T. Lohmann, B. Kozinsky, R. Liedtke, J. Ahmed, A. Kojic, A Critical Review of Li/Air Batteries, J. Electrochem. Soc. 159 (2) (2012) R1–S30, https://doi.org/10.1149/2.086202jes.
[3] J. Li, Z. Wang, Y. Wang, J. Wang, Phase-Field Study of Competitive Dendritic Growth of Converging Grains during Directional Solidification, Acta Mater. 60 (4) (2012) 1478–1493, https://doi.org/10.1016/j.actamat.2011.11.037.
[4] C. Zhongwei, C. Pei, F. Li, Effects of Melt Treatment on Dendrite Coherency of A357 Alloy, Adv. Mater. Res. 189–193 (2011) 3886–3890, https://doi.org/10.4028/www.scientific.net/AMR.189-193.3886.
[5] T. Yi-Da, Y. Chi-Yang, H. Chi-Chang, D. Jenq-Gong, Pulse Electroplating of Sn-Bi Alloys on Micropatterned Electrodes for Lead-Free Solder Bumping, J. Electrochem. Soc. 159 (2) (2012) 108–113, https://doi.org/10.1149/2.083202jes.
[6] C. Xinwei, C. Weixing, Saccharin Effects on Direct-Current Electroplating Nanocrystalline Ni-Cu Alloys, J. Electrochem. Soc. 155 (9) (2008) 133–139, https://doi.org/10.1149/1.2948362.
[7] K. Yan, J. Wang, S. Zhao, D. Zhou, B. Sun, Y. Cui, G. Wang, Temperature-Dependent Nucleation and Growth of Dendrite-Free Lithium Metal Anodes, Angew. Chemie Int. Ed. 58 (33) (2019) 11364–11368, https://doi.org/10.1002/anie.201905251.
[8] B.S. Vishnugopi, F. Hao, A. Verma, P.P. Mukherjee, Double-Edged Effect of Temperature on Lithium Dendrites, ACS Appl. Mater. Interfaces 12 (21) (2020) 23931–23938, https://doi.org/10.1021/acsami.0c0435510.1021/acsami.0c04355.s001.
[9] W. Liu, P. Liu, D. Mitlin, Tutorial Review on Structure – Dendrite Growth Relations in Metal Battery Anode Supports, Chem. Soc. Rev. 49 (20) (2020) 7284–7300, https://doi.org/10.1039/D0CS00867B.
[10] T. Zhang, J. Yang, Z. Xu, H. Li, Y. Guo, C. Liang, J. Wang, Suppressing Dendrite Growth of a Lithium Metal Anode by Modifying Conventional Polypropylene Separators with a Composite Layer, ACS Appl. Energy Mater. 3 (1) (2020) 506–513, https://doi.org/10.1021/acsaem.9b0176310.1021/acsaem.9b01763.s001.
[11] Jang, J.; Oh, J.; Jeong, H.; Kang, W.; Jo, C. A Review of Functional Separators for Lithium Metal Battery Applications. Mater. (Basel, Switzerland) 2020, 13 (20), 4625. https://doi.org/10.3390/ma13204625.
[12] A. Hagopian, M.-L. Doublet, J.-S. Filhol, Thermodynamic Origin of Dendrite Growth in Metal Anode Batteries, Energy Environ. Sci. 13 (12) (2020) 5186–5197, https://doi.org/10.1039/D0EE02665D.
[13] K. Wang, Solutions for Dendrite Growth of Electrodeposited Zinc, ACS Omega 5 (18) (2020) 10225–10227, https://doi.org/10.1021/acsomega.0c01485.

[14] S. Park, H.-J. Jin, Y.S. Yun, Advances in the Design of 3D-Structured Electrode Materials for Lithium-Metal Anodes, Adv. Mater. 32 (51) (2020) 2002193, https://doi.org/10.1002/adma.202002193.

[15] H.e. Liu, X.-B. Cheng, J.-Q. Huang, H. Yuan, Y. Lu, C. Yan, G.-L. Zhu, R. Xu, C.-Z. Zhao, L.-P. Hou, C. He, S. Kaskel, Q. Zhang, Controlling Dendrite Growth in Solid-State Electrolytes, ACS Energy Lett. 5 (3) (2020) 833–843, https://doi.org/10.1021/acsenergylett.9b02660.

[16] M. Golozar, A. Paolella, H. Demers, S. Savoie, G. Girard, N. Delaporte, R. Gauvin, A. Guerfi, H. Lorrmann, K. Zaghib, Direct Observation of Lithium Metal Dendrites with Ceramic Solid Electrolyte, Sci. Rep. 10 (1) (2020) 18410, https://doi.org/10.1038/s41598-020-75456-0.

[17] Z. Ahmad, Z. Hong, V. Viswanathan, Design Rules for Liquid Crystalline Electrolytes for Enabling Dendrite-Free Lithium Metal Batteries, Proc. Natl. Acad. Sci. 117 (43) (2020) 26672–26680, https://doi.org/10.1073/pnas.2008841117.

[18] H. Liu, X.-B. Cheng, Z. Jin, R. Zhang, G. Wang, L.-Q. Chen, Q.-B. Liu, J.-Q. Huang, Q. Zhang, Recent Advances in Understanding Dendrite Growth on Alkali Metal Anodes, EnergyChem 1 (1) (2019), 100003, https://doi.org/10.1016/j.enchem.2019.100003.

[19] Z. Ahmad, T. Xie, C. Maheshwari, J.C. Grossman, V. Viswanathan, M.A. Makeev, N. N. Rajput, Machine Learning Enabled Computational Screening of Inorganic Solid Electrolytes for Suppression of Dendrite Formation in Lithium Metal Anodes, ACS Cent. Sci. 4 (8) (2019) 58–69, https://doi.org/10.1021/acscentsci.8b00229.

[20] M.A. Makeev, N.N. Rajput, Computational Screening of Electrolyte Materials: Status Quo and Open Problems, Curr. Opin. Chem. Eng. 23 (2019) 58–69, https://doi.org/10.1016/j.coche.2019.02.008.

[21] M.-S. Park, Y.-S. Kang, D. Im, A High-Speed Screening Method by Combining a High-Throughput Method and a Machine-Learning Algorithm for Developing Novel Organic Electrolytes in Rechargeable Batteries, ECS Trans. 68 (2) (2015) 75–81, https://doi.org/10.1149/06802.0075ecst.

[22] K. Hatakeyama-Sato, T. Tezuka, Y. Nishikitani, H. Nishide, K. Oyaizu, Synthesis of Lithium-Ion Conducting Polymers Designed by Machine Learning-Based Prediction and Screening, Chem. Lett. 48 (2) (2018) 130–132, https://doi.org/10.1246/cl.180847.

[23] A.D. Sendek, E.D. Cubuk, E.R. Antoniuk, G. Cheon, Y.i. Cui, E.J. Reed, Machine Learning-Assisted Discovery of Solid Li-Ion Conducting Materials, Chem. Mater. 31 (2) (2019) 342–352, https://doi.org/10.1021/acs.chemmater.8b0327210.1021/acs.chemmater.8b03272.s001.

[24] Y. Liu, B. Guo, X. Zou, Y. Li, S. Shi, Machine Learning Assisted Materials Design and Discovery for Rechargeable Batteries, Energy Storage Mater. 31 (2020) 434–450, https://doi.org/10.1016/j.ensm.2020.06.033.

[25] L.D. Ellis, S. Buteau, S.G. Hames, L.M. Thompson, D.S. Hall, J.R. Dahn, A New Method for Determining the Concentration of Electrolyte Components in Lithium-Ion Cells, Using Fourier Transform Infrared Spectroscopy and Machine Learning, J. Electrochem. Soc. 165 (2) (2018) A256–A262, https://doi.org/10.1149/2.0861802jes.

[26] B.K. Wheatle, E.F. Fuentes, N.A. Lynd, V. Ganesan, Design of Polymer Blend Electrolytes through a Machine Learning Approach, Macromolecules 53 (21) (2020) 9449–9459, https://doi.org/10.1021/acs.macromol.0c0154710.1021/acs.macromol.0c01547.s001.

[27] A. Ishikawa, K. Sodeyama, Y. Igarashi, T. Nakayama, Y. Tateyama, M. Okada, Machine Learning Prediction of Coordination Energies for Alkali Group Elements in Battery Electrolyte Solvents, Phys. Chem. Chem. Phys. 21 (48) (2019) 26399–26405, https://doi.org/10.1039/C9CP03679B.

[28] B. He, S. Chi, A. Ye, P. Mi, L. Zhang, B. Pu, Z. Zou, Y. Ran, Q. Zhao, D.a. Wang, W. Zhang, J. Zhao, S. Adams, M. Avdeev, S. Shi, High-Throughput Screening Platform for Solid Electrolytes Combining Hierarchical Ion-Transport Prediction Algorithms, Sci. Data 7 (1) (2020), https://doi.org/10.1038/s41597-020-0474-y.

[29] M. Korth, Large-Scale Virtual High-Throughput Screening for the Identification of New Battery Electrolyte Solvents: Evaluation of Electronic Structure Theory Methods, Phys. Chem. Chem. Phys. 16 (17) (2014) 7919–7926, https://doi.org/10.1039/C4CP00547C.

[30] S. Huang, J.M. Cole, A Database of Battery Materials Auto-Generated Using ChemDataExtractor, Sci. Data 7 (1) (2020) 260, https://doi.org/10.1038/s41597-020-00602-2.

[31] J. Tan, A.M. Tartakovsky, K. Ferris, E.M. Ryan, Investigating the Effects of Anisotropic Mass Transport on Dendrite Growth in High Energy Density Lithium Batteries, J. Electrochem. Soc. 163 (2) (2016) A318–A327, https://doi.org/10.1149/2.0951602jes.

[32] K. Goossens, K. Lava, C.W. Bielawski, K. Binnemans, Ionic Liquid Crystals: Versatile Materials, Chem. Rev. 116 (8) (2016) 4643–4807, https://doi.org/10.1021/cr400334b10.1021/cr400334b.s001.

[33] J. Tan, E.M. Ryan, Computational Study of Electro-Convection Effects on Dendrite Growth in Batteries, J. Power Sources 323 (2016) 67–77, https://doi.org/10.1016/j.jpowsour.2016.05.012.

[34] J. Tan, E.M. Ryan, Structured Electrolytes to Suppress Dendrite Growth in High Energy Density Batteries, Int. J. Energy Res. 40 (13) (2016) 1800–1810, https://doi.org/10.1002/er.v40.1310.1002/er.3560.

[35] Axenov, K. V; Laschat, S. Thermotropic Ionic Liquid Crystals. Mater. (Basel, Switzerland) 2011, 4 (1), 206–259. https://doi.org/10.3390/ma4010206.

[36] A.E. Bradley, C. Hardacre, J.D. Holbrey, S. Johnston, S.E.J. McMath, M. Nieuwenhuyzen, Small-Angle X-Ray Scattering Studies of Liquid Crystalline 1-Alkyl-3-Methylimidazolium Salts, Chem. Mater. 14 (2) (2002) 629–635, https://doi.org/10.1021/cm010542v.

[37] L.M. Antill, M.M. Neidhardt, J. Kirres, S. Beardsworth, M. Mansueto, A. Baro, S. Laschat, Ionic Liquid Crystals Derived from Guanidinium Salts: Induction of Columnar Mesophases by Bending of the Cationic Core, Liq. Cryst. 41 (7) (2014) 976–985, https://doi.org/10.1080/02678292.2014.896052.

[38] F. Lo Celso, I. Pibiri, A. Triolo, R. Triolo, A. Pace, S. Buscemi, N. Vivona, Study on the Thermotropic Properties of Highly Fluorinated 1{,}2{,}4-Oxadiazolylpyridinium Salts and Their Perspective Applications as Ionic Liquid Crystals, J. Mater. Chem. 17 (12) (2007) 1201–1208, https://doi.org/10.1039/B615190F.

[39] M. Butschies, M.M. Neidhardt, M. Mansueto, S. Laschat, S. Tussetschläger, Synthesis of Guanidinium-Sulfonimide Ion Pairs: Towards Novel Ionic Liquid Crystals, Beilstein J. Org. Chem. 9 (2013) 1093–1101.

[40] S.-C. Luo, S. Sun, A.R. Deorukhkar, J.-T. Lu, A. Bhattacharyya, I.J.B. Lin, Ionic Liquids and Ionic Liquid Crystals of Vinyl Functionalized Imidazolium Salts, J. Mater. Chem. 21 (6) (2011) 1866–1873, https://doi.org/10.1039/C0JM02875D.

[41] T. Mukai, M. Yoshio, T. Kato, H. Ohno, Self-Assembled N-Alkylimidazolium Perfluorooctanesulfonates, Chem. Lett. 34 (3) (2005) 442–443, https://doi.org/10.1246/cl.2005.442.

[42] T. Mukai, M. Yoshio, T. Kato, M. Yoshizawa, H. Ohno, Anisotropic Ion Conduction in a Unique Smectic Phase of Self-Assembled Amphiphilic Ionic Liquids, Chem. Commun. 10 (2005) 1333–1335, https://doi.org/10.1039/B414631J.

[43] T. Mukai, M. Yoshio, T. Kato, M. Yoshizawa-Fujita, H. Ohno, Self-Organization of Protonated 2-Heptadecylimidazole as an Effective Ion Conductive Matrix, Electrochemistry 73 (8) (2005) 623–626, https://doi.org/10.5796/electrochemistry.73.623.

[44] J. Sakuda, M. Yoshio, T. Ichikawa, H. Ohno, T. Kato, 2D Assemblies of Ionic Liquid Crystals Based on Imidazolium Moieties: Formation of Ion-Conductive Layers, New J. Chem. 39 (6) (2015) 4471–4477, https://doi.org/10.1039/C5NJ00085H.

[45] H. Shimura, M. Yoshio, K. Hoshino, T. Mukai, H. Ohno, T. Kato, Noncovalent Approach to One-Dimensional Ion Conductors: Enhancement of Ionic Conductivities in Nanostructured Columnar Liquid Crystals, J. Am. Chem. Soc. 130 (5) (2008) 1759–1765, https://doi.org/10.1021/ja0775220.

[46] G.F. Starkulla, S. Klenk, M. Butschies, S. Tussetschläger, S. Laschat, Towards Room Temperature Ionic Liquid Crystals: Linear versus Bent Imidazolium Phenylpyrimidines, J. Mater. Chem. 22 (41) (2012) 21987–21997, https://doi.org/10.1039/C2JM34595A.

[47] C.M. Gordon, J.D. Holbrey, A.R. Kennedy, K.R. Seddon, Ionic Liquid Crystals: Hexafluorophosphate Salts, J. Mater. Chem. 8 (12) (1998) 2627–2636, https://doi.org/10.1039/a806169f.

[48] X. Wang, M. Sternberg, F.T.U. Kohler, B.U. Melcher, P. Wasserscheid, K. Meyer, Long-Alkyl-Chain-Derivatized Imidazolium Salts and Ionic Liquid Crystals with Tailor-Made Properties, RSC Adv. 4 (24) (2014) 12476–12481, https://doi.org/10.1039/C3RA47250G.

[49] Z. Wei, X. Wei, X. Wang, Z. Wang, J. Liu, Ionic Liquid Crystals of Quaternary Ammonium Salts with a 2-Hydroxypropoxy Insertion Group, J. Mater. Chem. 21 (19) (2011) 6875–6882, https://doi.org/10.1039/C1JM10236B.

[50] E. Westphal, D.H.d. Silva, F. Molin, H. Gallardo, Pyridinium and Imidazolium 1{,}3{,}4-Oxadiazole Ionic Liquid Crystals: A Thermal and Photophysical Systematic Investigation, RSC Adv. 3 (18) (2013) 6442, https://doi.org/10.1039/c3ra23456h.

[51] G. Cavallo, G. Terraneo, A. Monfredini, M. Saccone, A. Priimagi, T. Pilati, G. Resnati, P. Metrangolo, D.W. Bruce, Superfluorinated Ionic Liquid Crystals Based on Supramolecular, Halogen-Bonded Anions, Angew. Chemie Int. Ed. 55 (21) (2016) 6300–6304, https://doi.org/10.1002/anie.201601278.

[52] S. Yazaki, M. Funahashi, J. Kagimoto, H. Ohno, T. Kato, Nanostructured Liquid Crystals Combining Ionic and Electronic Functions, J. Am. Chem. Soc. 132 (22) (2010) 7702–7708, https://doi.org/10.1021/ja101366x.

[53] A. Yildirim, P. Szymoniak, K. Sentker, M. Butschies, A. Bühlmeyer, P. Huber, S. Laschat, A. Schönhals, Dynamics and Ionic Conductivity of Ionic Liquid Crystals Forming a Hexagonal Columnar Mesophase, Phys. Chem. Chem. Phys. 20 (8) (2018) 5626–5635, https://doi.org/10.1039/C7CP08186C.

[54] M. Yoshio, T. Kagata, K. Hoshino, T. Mukai, H. Ohno, T. Kato, One-Dimensional Ion-Conductive Polymer Films: Alignment and Fixation of Ionic Channels Formed by Self-Organization of Polymerizable Columnar Liquid Crystals, J. Am. Chem. Soc. 128 (16) (2006) 5570–5577, https://doi.org/10.1021/ja0606935.

[55] M. Yoshio, T. Ichikawa, H. Shimura, T. Kagata, A. Hamasaki, T. Mukai, H. Ohno, T. Kato, Columnar Liquid-Crystalline Imidazolium Salts. Effects of Anions and Cations on Mesomorphic Properties and Ionic Conductivities, Bull. Chem. Soc. Jpn. 80 (9) (2007) 1836–1841.

[56] W. YU, H. PENG, H. ZHANG, X. ZHOU, Synthesis and Mesophase Behaviour of Morpholinium Ionic Liquid Crystals, Chinese J. Chem. 27 (8) (2009) 1471–1475, https://doi.org/10.1002/cjoc.v27:810.1002/cjoc.200990247.

[57] J.Y.Z. Chiou, J.N. Chen, J.S. Lei, I.J.B. Lin, Ionic Liquid Crystals of Imidazolium Salts with a Pendant Hydroxyl Group, J. Mater. Chem. 16 (29) (2006) 2972–2977, https://doi.org/10.1039/B600045B.

[58] Y. Haramoto, Y. Akiyama, R. Segawa, S. Ujiie, M. Nanasawa, New 1{,}3-Oxathiane Type Ionic Liquid Crystal Compounds, J. Mater. Chem. 8 (2) (1998) 275–276, https://doi.org/10.1039/A707622C.

[59] D. Haristoy, D. Tsiourvas, Effect of Counterions on the Thermotropic and Thermochromic Properties of Ionic Liquid Crystals, Liq. Cryst. 31 (5) (2004) 697–703, https://doi.org/10.1080/02678290410001675110.

[60] X. Feng, M.E. Tousley, M.G. Cowan, B.R. Wiesenauer, S. Nejati, Y. Choo, R. D. Noble, M. Elimelech, D.L. Gin, C.O. Osuji, Scalable Fabrication of Polymer Membranes with Vertically Aligned 1 Nm Pores by Magnetic Field Directed Self-Assembly, ACS Nano 8 (12) (2014) 11977–11986, https://doi.org/10.1021/nn505037b.

[61] J. Fouchet, L. Douce, B. Heinrich, R. Welter, A. Louati, A Convenient Method for Preparing Rigid-Core Ionic Liquid Crystals, Beilstein J. Org. Chem. 5 (2009) 51, https://doi.org/10.3762/bjoc.5.51.

[62] K. Goossens, K. Lava, P. Nockemann, K. Van Hecke, L. Van Meervelt, P. Pattison, K. Binnemans, T. Cardinaels, Pyrrolidinium Ionic Liquid Crystals with Pendant Mesogenic Groups, Langmuir 25 (10) (2009) 5881–5897, https://doi.org/10.1021/la900048h.
[63] H. Yoshizawa, T. Mihara, N. Koide*, THERMAL PROPERTIES AND IONIC CONDUCTIVITY OF IMIDAZOLIUM SALT DERIVATIVES HAVING A CALAMITIC MESOGEN, Mol. Cryst. Liq. Cryst. 423 (1) (2004) 61–72, https://doi.org/10.1080/15421400490502481.
[64] D. Holbrey, J.; R. Seddon, K. The Phase Behaviour of 1-Alkyl-3-Methylimidazolium Tetrafluoroborates; Ionic Liquids and Ionic Liquid Crystals. J. Chem. Soc.{,} Dalt. Trans. 1999, No. 13, 2133–2140. https://doi.org/10.1039/A902818H.
[65] T. Ichikawa, M. Yoshio, A. Hamasaki, T. Mukai, H. Ohno, T. Kato, Self-Organization of Room-Temperature Ionic Liquids Exhibiting Liquid-Crystalline Bicontinuous Cubic Phases: Formation of Nano-Ion Channel Networks, J. Am. Chem. Soc. 129 (35) (2007) 10662–10663, https://doi.org/10.1021/ja0740418.
[66] T. Ichikawa, M. Yoshio, A. Hamasaki, S. Taguchi, F. Liu, X. Zeng, G. Ungar, H. Ohno, T. Kato, Induction of Thermotropic Bicontinuous Cubic Phases in Liquid-Crystalline Ammonium and Phosphonium Salts, J. Am. Chem. Soc. 134 (5) (2012) 2634–2643, https://doi.org/10.1021/ja209010m.
[67] D. Kuo, B. Soberats, K.R.S. Kumar, M. Yoshio, T. Ichikawa, H. Ohno, X. Zeng, G. Ungar, T. Kato, Switching of Ionic Conductivities in Columnar Liquid-Crystalline Anilinium Salts: Effects of Alkyl Chains{,} Ammonium Cations and Counter Anions on Thermal Properties and Switching Temperatures, Mol. Syst. Des. Eng. 4 (2) (2019) 342–347, https://doi.org/10.1039/C8ME00099A.
[68] K. Lava, K. Binnemans, T. Cardinaels, Piperidinium, Piperazinium and Morpholinium Ionic Liquid Crystals, J. Phys. Chem. B 113 (28) (2009) 9506–9511, https://doi.org/10.1021/jp903667e.
[69] H. Yamada, C. Liu, S. Wu, Y. Koyama, S. Ju, J. Shiomi, J. Morikawa, R. Yoshida, Predicting Materials Properties with Little Data Using Shotgun Transfer Learning, ACS Cent. Sci. 5 (10) (2019) 1717–1730, https://doi.org/10.1021/acscentsci.9b00804.
[70] V. Venkatraman, S. Evjen, K. Chellappan Lethesh, The Ionic Liquid Property Explorer: An Extensive Library of Task-Specific Solvents, Data 4 (2) (2019) 88, https://doi.org/10.3390/data4020088.
[71] Chollet, F. Keras. GitHub repository. GitHub 2015.
[72] Kaycee Low, Rika Kobayashi, Ekaterina I. Izgorodina, The Effect of Descriptor Choice in Machine Learning Models for Ionic Liquid Melting Point Prediction, J. Chem. Phys. 153 (10) (2020) 104101, https://doi.org/10.1063/5.0016289.
[73] Goh, G. B.; Siegel, C.; Vishnu, A.; Hodas, N. O.; Baker, N. Chemception: A Deep Neural Network with Minimal Chemistry Knowledge Matches the Performance of Expert-Developed QSAR/QSPR Models. 2017.
[74] G.B. Goh, C. Siegel, A. Vishnu, N.O. Hodas, Using Rule-Based Labels for Weak Supervised Learning, A ChemNet for Transferable Chemical Property Prediction. (2017).
[75] S. Zhong, J. Hu, X. Yu, H. Zhang, Molecular Image-Convolutional Neural Network (CNN) Assisted QSAR Models for Predicting Contaminant Reactivity toward OH Radicals: Transfer Learning, Data Augmentation and Model Interpretation, Chem. Eng. J. 408 (2021), 127998, https://doi.org/10.1016/j.cej.2020.127998.
[76] N.J. Lentelink, S. Palkovits, Transfer Learning as Tool to Enhance Predictions of Molecular Properties Based on 2D Projections, Adv. Theory Simulations 3 (10) (2020) 2000148, https://doi.org/10.1002/adts.202000148.
[77] I. Cortés-Ciriano, A. Bender, KekuleScope: Prediction of Cancer Cell Line Sensitivity and Compound Potency Using Convolutional Neural Networks Trained on Compound Images, J. Cheminform. 11 (1) (2019) 41, https://doi.org/10.1186/s13321-019-0364-5.
[78] H.Y.D. Sigaki, E.K. Lenzi, R.S. Zola, M. Perc, H.V. Ribeiro, Learning Physical Properties of Liquid Crystals with Deep Convolutional Neural Networks, Sci. Rep. 10 (1) (2020) 7664, https://doi.org/10.1038/s41598-020-63662-9.
[79] Landrum, G. RDKit: Open-Source Cheminformatics.
[80] V. Venkatraman, S. Evjen, H.K. Knuutila, A. Fiksdahl, B.K. Alsberg, Predicting Ionic Liquid Melting Points Using Machine Learning, J. Mol. Liq. 264 (2018) 318–326, https://doi.org/10.1016/j.molliq.2018.03.090.
[81] Z. Wang, Z. Dai, B. Póczos, J. Carbonell, Characterizing and Avoiding Negative Transfer. (2018).
[82] G. Bradski, The OpenCV Library, Dr. Dobb's J. Softw Tools, 2000.
[83] Zhenqin Wu, Bharath Ramsundar, Evan N. Feinberg, Joseph Gomes, Caleb Geniesse, Aneesh S. Pappu, Karl Leswing, Vijay Pande, Machine Learning. 9 (2) (2018) 513–530.
[84] D. Duvenaud, D. Maclaurin, J. Aguilera-Iparraguirre, R. Gómez-Bombarelli, T. Hirzel, A. Aspuru-Guzik, R.P. Adams, Convolutional Networks on Graphs for Learning Molecular Fingerprints. (2015).